Physicochem. Probl. Miner. Process., 54(3), 2018, 763-770

http://www.journalssystem.com/ppmp

Physicochemical Problems of Mineral Processing

ISSN 1643-1049

Received December 18, 2017; reviewed; accepted February 8, 2018

The surface features of activated stibnite surface with copper or lead ion

Qinbo Cao [1], Yu Huang [2], Heng Zou [3], Shuming Wen [1]

[1] State Key Laboratory of Complex Nonferrous Metal Resources Clean Utilization, Kunming, 650093, Yunnan, PR China

[2] Faculty of Land Resources Engineering, Kunming University of Science and Technology, Kunming 650093, Yunnan, PR China

[3] Faculty of Information Engineering and Automation, Kunming University of Science and Technology, Kunming, 650093, Yunnan, PR China

Corresponding authors: cabdxx@163.com (Qinbo Cao)

Abstract: Cu^{2+} and Pb^{2+} are widely used as activators for the flotation of stibnite. In this work, by the treatment of Cu^{2+} or Pb^{2+}, the activation product and the thickness of activation layer on the stibnite surface were both investigated. Based on the flotation results, zeta potential analysis and X-ray photoelectron spectroscopy (XPS) study, it was found that Cu^{2+} was reduced to Cu^{+} at the stibnite surface and a layer of Cu_2S was formed at the surface. While, a PbS layer presenting at the stibnite surface is responsible for the activation flotation of stibnite with Pb^{2+}. Time of flight secondary ion mass spectrometry (TOF-SIMS) analysis further implies that, when stibnite was activated with 5×10^{-5} mol/dm^3 of $CuSO_4$ or $Pb(NO_3)_2$, the thickness of Cu_2S layer on the Cu-activated surface was close to 2.7 nm, while the thickness of PbS layer was about 1.8 nm on the Pb-activated surface.

Keywords: stibnite, flotation, activation, active layer

1. Introduction

Antimony is an important metal that is widely used in the production of alloys, flame retardants and other fields (Anderson, 2012). China, the biggest mined production country, provides the world with about 90% of antimony resources (Anderson, 2012). Stibnite, jamesonite are the main sources of antimony (Lager and Forssberg, 1989; Lager and Forssberg, 2015). Stibnite, as the most important antimony mineral, is commonly floated with xanthates and activator at natural pH to be separated from other gangue minerals (Huang, 1987).

Copper sulfate and lead nitrate are efficient activators in the flotation of stibnite and other minerals (Xu et al., 1991; Dai et al., 2009). Peng et al. investigated the flotation mechanism of pyrite activated by Cu^{2+} and Pb^{2+} (Peng and Grano, 2010). Li et al. studied the effect of Pb^{2+} on the adsorption capacity of salicylhydroxamic acid on rutile surface (Li et al., 2016). Sarvaramini A et al. examined the species on sphalerite surface after lead-activation (Sarvaramini et al., 2016). Previous study reveal that Cu^{2+} or Pb^{2+} transfers from solution to the mineral surface forming a new active layer (Sui et al., 1997).

It has been demonstrated that the activation flotation of stibnite with Cu^{2+} or Pb^{2+} ion depends on the formation of new activation layer on the stibnite surface (Solozhenkin et al., 1991). However, the previous work focused on the effect of Cu^{2+} or Pb^{2+} concentration on the flotation performance of stibnite. Less effort was made to measure the thickness of activation layer on the stibnite surface.

Time of flight secondary ion mass spectrometry (TOF-SIMS) is a powerful tool to analyze the chemical species and their distributions on a mineral surface, with an extremely high sensitivity (Chelgani et al., 2013; Chelgani and Hart, 2014). TOF-SIMS uses bismuth ion beam to bombard a mineral surface, by which the charged secondary ions are generated from the surface. Each secondary ion has a distinctive mass to charge ratio, therefore the species on the mineral surface can be identified by TOF-

http://dx.doi.org/10.5277/ppmp1884

SIMS. T.N. Khmeleva et al. used TOF-SIMS to investigate the species distribution of sulphur oxides on copper-activated pyrites (Khmeleva et al., 2003). Mao D et al. employed TOF-SIMS to study two-dimensional (2D) chemical distributions of impurities in CdTe samples (Mao et al., 2016). Despite the 2D distribution property, TOF-SIMS can provide the three-dimensional (3D) distribution of chemical species on a sample surface with a certain depth. S.G. Alberici et al. had investigated the inter diffusion properties and distribution of the Ti in chalcogenides by TOF-SIMS depth profile characterization (Alberici et al., 2004). Thomas, et al. successfully used TOF-SIMS depth profile to provide 3D chemical image of the interface between poly (3,4-ethylene-dioxythiophene): polystyrenesulfonate (PEDOT: PSS) and SiO_x/Si in a hybrid solar cell (Thomas et al., 2013).

The objective of this paper is to investigate the surface products and their 3D distribution on the stibnite surface by the activation of Cu^{2+} or Pb^{2+}. Firstly, micro-flotation and zeta potential techniques were used to study the flotation performance of stibnite activated by Cu^{2+}or Pb^{2+}. XPS was further employed to identify the activation products at the stibnite surface. The thickness of active layers was determined by the TOF-SIMS technique, which is important to understand the activation flotation of stibnite with Pb^{2+} and Cu^{2+}.

2. Material and methods

2.1 Stibnite samples and reagents

The stibnite pebbles were obtained from Dali, Yunnan provinces, China. The X-ray diffraction (XRD) pattern of the sample shows that the purity of stibnite was higher than 98% (Fig.1), and further chemical analysis suggests that the stibnite sample contains 71.60% of Sb and 28.27% of S. Deionized (DI) water was used in the all experiments. $Pb(NO_3)_2$, $CuSO_4$, HCl, NaOH, KNO_3 and butyl xanthate were AR grade and purchased from Sinopharm Chemical Reagent Co., Ltd. Pine oil was provided by Hunan Minzhu Flotation Reagents Co., Ltd.

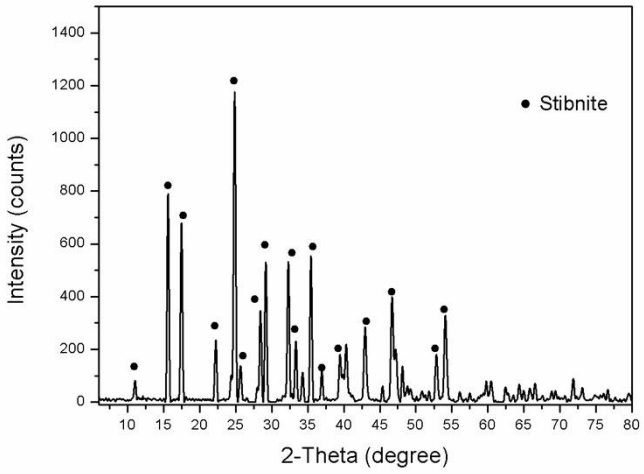

Fig. 1. XRD pattern of the pure stibnite sample

2.2 Micro-flotation tests

Micro-flotation tests were conducted in a 40 cm^3 of XFG cell, using 2 g of mineral (-200 mesh +250 mesh). The pulp was stirred for 3 min after the addition of $CuSO_4$ or $Pb(NO_3)_2$, after which butyl xanthate (BX) was added into the pulp (1×10^{-5} mol/dm^3). Pine oil was used as the forther with a concentration of 25 mg/L. The condition times for BX and pine oil were both 2 min. The flotation test was performed for 1 min using air at a flow rate of 20 cm^3/min. Each test was repeated three times.

2.3 Electrokinetic analysis

A Nano ZSP from Malvern Instruments Ltd. was used to measure the electrophoretic mobility of the stibnite in solutions. The zeta potentials were further calculated by the software of the instrument using the Smoluchowski equation. During the measurement, 1×10^{-3} mol/dm^3 of KNO_3 was used as supporting

electrolyte solution. 0.1 g of mineral powder (-5 μm) was transferred to a beaker with 100mL of solutions with desired concentrations of activator. The suspension was stirred for 3 min with a magnetic stirrer. Then, 10 cm^3 of suspension was taken for the test. The average value of 40 measurements was reported.

2.4 X-ray photoelectron spectroscopy (XPS)

A PHI 5000 Versa Probe II equipped with an Al target was used to obtained the XPS spectra. The incident radiation was monochromatic Al Ka X-rays (1486.6 eV) at 150W. 1 g of stibnite sample (-5 μm) was conditioned with 100 cm^3 $CuSO_4$ or $Pb(NO_3)_2$ solution for 3 min. The sample was further air-dried for the XPS study. The XPS spectra were corrected using the main line of the C1s peak, with an assigned binding energy of 284.8 eV. The spectra were further fitted using Gaussian-Lorenztian equation.

2.5 Time of flight secondary ion mass spectrometry (TOF-SIMS) analysis

TOF-SIMS experiments were conducted with a TOF-SIMS 5 instrument from ION-TOF GmbH, Germany. The surface imaging analysis were performed with an 30 keV of Bi_3^+ primary ion with the spectrometry model. The analysis area was 100×100 μm^2 with a measurement time of 120 ms. In the case of depth profiling study, the O^{2+} beam was used in the non-interlaced model (1 s sputter time, 0.5 s pause) to record the depth profiles of selected ions on the stibnite surface. The parameters for the primary beam was same to that in the surface imaging analysis. The sputter crater dimension was 300×300 μm^2 and the Bi^+ beam was rastered over an 100×100 μm^2 area for the analysis. To prepare samples for TOF-SIMS analysis, the stibnite pebbles were polished and then were immersed in the $CuSO_4$ or $Pb(NO_3)_2$ solution for 3 min. The treated samples were rinsed with DI water and air-dried before the analysis.

3. Results and discussion

3.1 Micro-flotation experiment

Micro-flotation tests were employed to assess the influence of $CuSO_4$ and $Pb(NO_3)_2$ on the flotation of stibnite. Without any activator, the recovery was only 63.27% with 1×10^{-5} mol/dm^3 of BX (Fig. 2). Adding $CuSO_4$ or $Pb(NO_3)_2$ into the slurry favored the flotation of stibnite. With 5×10^{-5} mol/dm^3 of $CuSO_4$, the recovery reached about 75%. However, the further increase in $CuSO_4$ concentration deteriorated the stibnite flotation, resulting in an decrease in recovery comparing with that with 5×10^{-5} mol/dm^3 of $CuSO_4$. In the solution with a high Cu^{2+} concentration, BX ion may react with Cu^{2+} in the solution prior to adsorbing at the stibnite surface. Thus, the concentration of BX in the slurry is consumed, which cannot generate a satisfied recovery.

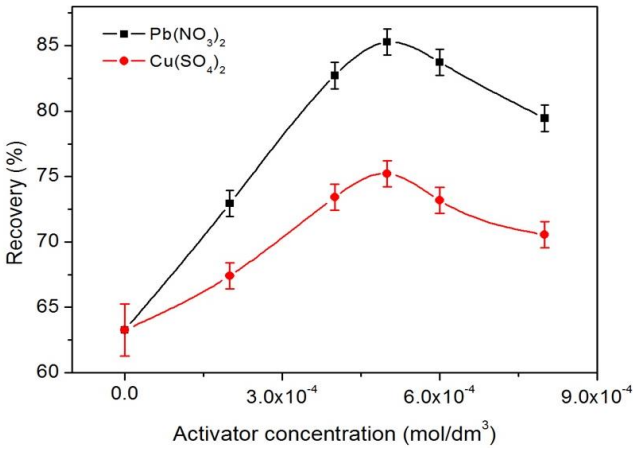

Fig. 2. Effect of activators concentration on stibnite flotation (concentration of BX is 1×10^{-5}mol/dm^3 and the pH is 6.5)

The flotation behavior of stibnite activated with $Pb(NO_3)_2$ was similar to that with $CuSO_4$. The stibnite recovery peaked at 5×10^{-5} mol/dm^3 of $Pb(NO_3)_2$. Perhaps to the same reason to that in the $CuSO_4$

solution, high dosage of $Pb(NO_3)_2$ (>5×10^{-5} mol/dm^3) was unfavorable for the stibnite flotation. Noted that the stibnite recovery with $Pb(NO_3)_2$ was higher than that with $CuSO_4$ at the same concentration, suggesting that $Pb(NO_3)_2$ is more efficient for the activation flotation of stibnite. This observation is in line with the previous reports (Huang and Wang, 1987; Solozhenkin et al., 1991).

3.2 Zeta potential analysis

The zeta potentials of stibnite depending on $CuSO_4$ and $Pb(NO_3)_2$ concentration at the pH of 6.5 are shown in Fig. 3. In DI water, the zeta potential of stibnite was -22.1 mV. After treated with $CuSO_4$ solution, the zeta potential of stibnite increased with the increasing in $CuSO_4$ concentration. With 1×10^{-4} mol/dm^3 of $CuSO_4$, the zeta potential of stibnite increased to -0.9 mV. Such results indicate that positive copper species adsorbed onto the stibnite surface. At the pH of 6.5, the dominant species of copper in 5×10^{-5} mol/dm^3 $CuSO_4$ solution is Cu^{2+} (4.67×10^{-5} mol/dm^3). It is expected that the adsorption of Cu^{2+} on the stibnite surface leads to an increase in zeta potential of stibnite.

Similar results were found for the stibnite in $Pb(NO_3)_2$ solutions. The addition of $Pb(NO_3)_2$ also increased the zeta potential of stibnite. While, it was found that the zeta potential with $Pb(NO_3)_2$ was close to that with $CuSO_4$ at the same dosage. For each examined dosage, the difference in zeta potentials (mean value) with two activators was less than 3 mV. At the pH of 6.5, the dominant species of lead in 5×10^{-5} mol/dm^3 of $Pb(NO_3)_2$ solution is Pb^{2+} ion (4.2×10^{-5}mol/dm^3). The positive Pb^{2+} may adsorb onto the negatively charged stibnite surface, resulting in an increase in the zeta potential of stibnite.

Above zeta potential results imply that Cu^{2+} or Pb^{2+} could adsorb onto the stibnite surface. XPS was further used to identify the activation products at the stibnite surface in the following part.

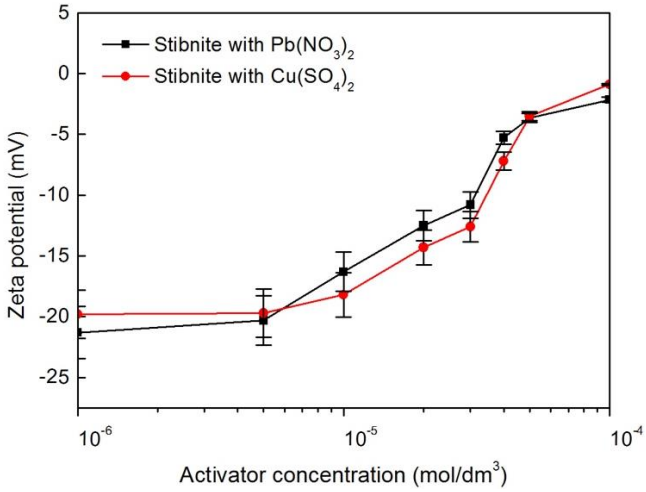

Fig. 3. Effect of $CuSO_4$ and $Pb(NO_3)_2$ concentration on zeta potential of stibnite at the pH of 6.5

3.3 X-ray photoelectron spectroscopy (XPS)

XPS can be used to analysis the chemical composition on a mineral surface according to the binding energy of each element's internal electrons. Fig. 4 displays the XPS spectra of stibnite conditioned with 5×10^{-5} mol/dm^3 of $CuSO_4$ or $Pb(NO_3)_2$ solution.

In the case of Cu-activated stibnite surface, the peaks of Cu 2p were observed in the XPS spectrum (Fig. 4a). It demonstrated that positive copper species adsorbed onto the stibnite surface after the Cu-activation, which supports the above the zeta potential results. A detail scan further revealed that the binding energies of Cu $2p_{3/2}$ and Cu $2p_{1/2}$ were 932.58 eV and 952.48 eV (Fig. 4b). Such Cu $2p_{3/2}$ and Cu $2p_{1/2}$ peaks should be assigned to the Cu^+ species in Cu_2S (Jiang et al., 2015). It appears that the Cu^{2+} interacted with the S atom at the stibnite surface and was reduced to Cu^+. As a result, new activation layer of Cu_2S formed at the stibnite surface. As for the Pb-activated stibnite surface, peaks of Pb 4f occurred in the XPS spectrum (Fig. 4c). The binding energies of Pb $4f_{7/2}$ and Pb $4f_{5/2}$, were 137.7 eV and 142.56 eV respectively (Fig. 4d), which can be attributed to the Pb^{2+} species in PbS (Wang et al., 2007). Such results imply that the PbS layer was formed at the Pb-activated stibnite surface.

The above XPS results indicate that Cu_2S layer formed at the stibnite surface by the activation of Cu^{2+} ion. While, in terms of the activation by Pb^{2+}, PbS layer could be generated on the stibnite surface. Such activation layers improved the floatability of stibnite.

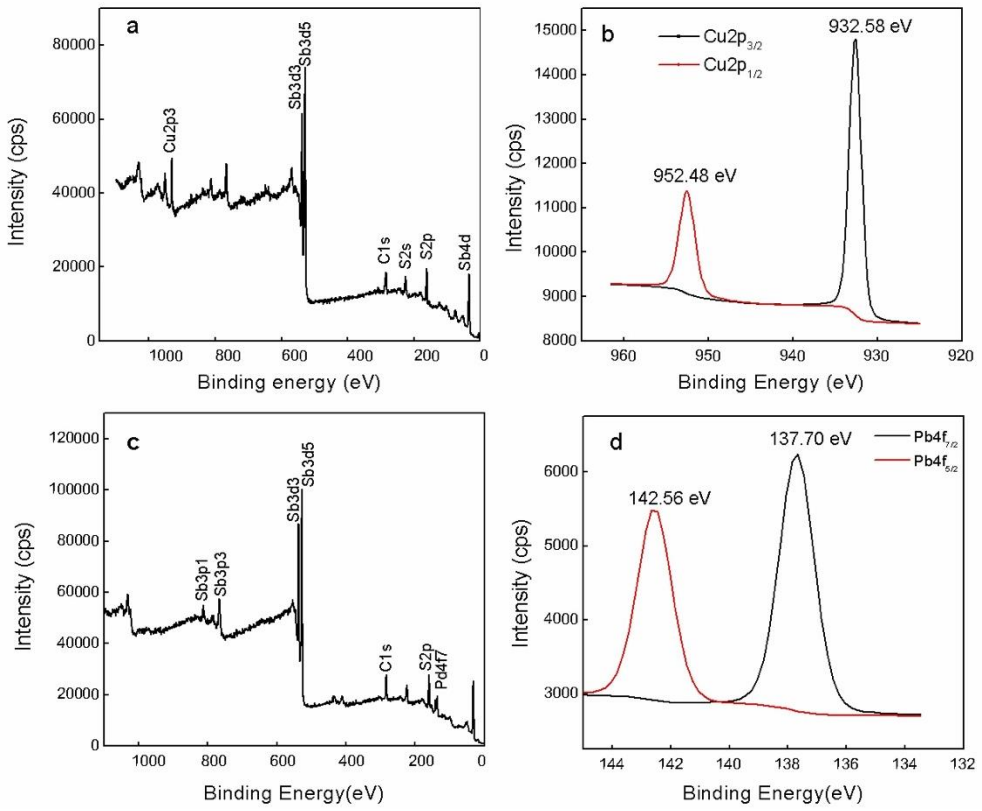

Fig. 4. XPS spectra for the stibnite surface treated with 5×10^{-5} mol/dm^3 $CuSO_4$ (a, b) and 5×10^{-5} mol/dm^3 $Pb(NO_3)_2$ (c, d)

3.4 TOF-SIMS analysis

3.4.1 Surface chemical analysis with TOF-SIMS

To further investigate the thickness of activation layer on the stibnite surface, TOF-SIMS technique was used to obtain the 3D distribution of ion-species on the stibnite surface.

For the natural stibnite, Sb^+, SbS^+ and Sb_2S^+ were detected as shown in Fig. 5a. In the case of Cu-activated surface, Cu^+, CuS^+ and Cu_2S^+ were measured, Fig. 5a. While the signals of other fragments related to Sb were weakened to some degree. The XPS results shows that a layer of Cu_2S formed at the Cu-activated stibnite surface. It is obvious that the Cu^+, CuS^+ and Cu_2S^+ signals came from the Cu_2S layer. It was noticed that the intensity of Cu^+ signal was much stronger than that of Cu_2S^+ fragment. It seems that the Cu-S bond of Cu_2S was broken when the Cu_2S layer was bombarded by the bismuth primary ion beam. Thus, the signal intensity of Cu^+ was relative stronger. On the Pb-activated surface, fragments of Pb^+ and PbS^+ were detected by the TOF-SIMS (Fig. 5b). The measured PbS^+ fragment support the XPS result that PbS layer presented at the Pb-activated surface. Again, since the Pb-S bond may be dissociated during the measurement, the intensity of PbS^+ was weaker than that of Pb^+.

We further evaluated the overlap images of Cu^+/Pb^+ and SbS^+ on the activated stibnite surface. The Cu^+ and Pb^+ ions come from the Cu_2S and PbS on the stibnite surface. Thus, their distribution on the stibnite surface can be used to analysis the distribution of Cu_2S and PbS on the surface.

Fig. 6 illustrates the overlay images of selected fragments on the Cu-activated stibnite surface and Pb-activated surface. On the Cu-activated surface, Cu^+ ion almost evenly distributed on the surface (Fig. 6a). Similar result is found for the Pb-activated surface, at where Pb^+ ion was well distributed on the stibnite surface (Fig. 6b). It seems that the stibnite surface was coated compactly by a layer of Cu_2S or PbS. With regard to the formation of active layer on the stibnite surface, two types of reactions may be

involved. First, Cu^{2+} or Pb^{2+} can directly bind with the S atom on the stibnite surface. On the other hand, it is also believed these ions also could migrate into a relative deeper layer of stibnite surface (Solozhenkin et al., 1991). In both events, a Cu_2S or PbS layer with certain thickness occurs on the stibnite surface.

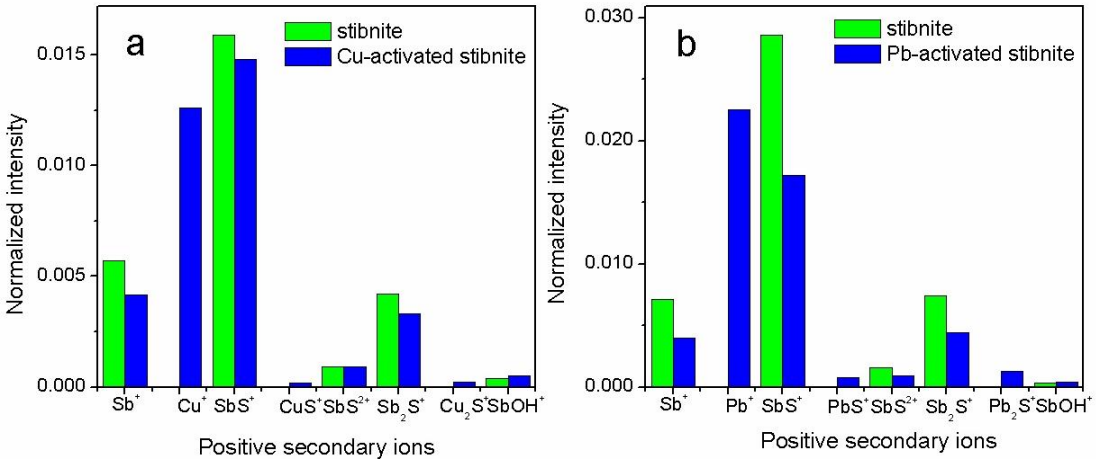

Fig. 5. Positive secondary ions spectra of natural stibnite and stibnite treated with 5×10^{-5} mol/dm^3 $CuSO_4$ (a) and $Pb(NO_3)_2$ (b)

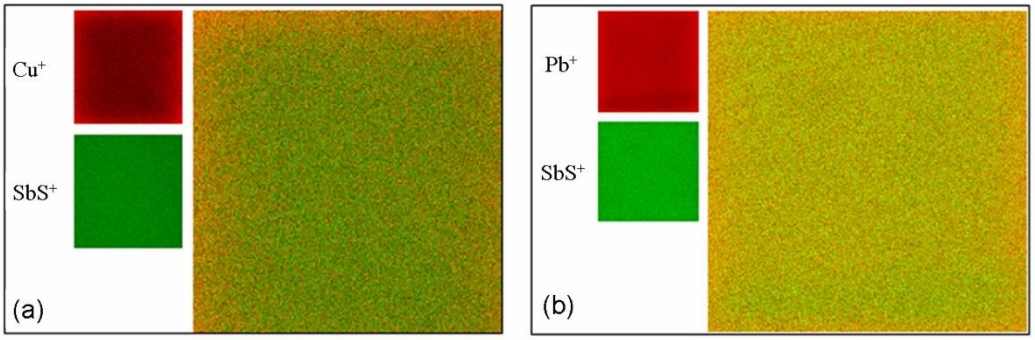

Fig. 6. Overlay images of Cu^+ (red) and SbS^+ (green) on the Cu-activated surface and Pb^+ (red) and SbS^+ (green) on the Pb-activated surface

3.4.2 Depth profiles and 3D analysis

Here we applied the TOF-SIMS with depth profiling to study the thickness of active layer on the stibnite surface. The positive secondary ions of Cu^+ and Pb^+ were used to locate the active layer during the depth profiling, since Cu^+ and Pb^+ are the most abundant fragments of active layer (Cu_2S layer, PbS layer) exposed to the probing beam.

The depth profiles of Cu^+ and Pb^+ from treated stibnite-surfaces were presented in Fig. 7. On the Cu-activated surface, the Cu^+ intensity drastically reduced with the increasing in measured depth. At 2.7 nm of depth, the intensity was about 11% of the maximal intensity (209954 cps), which may suggest that the Cu_2S layer has been punctured. This result shows that the thickness of Cu_2S layer was about 2.7 nm. For the Pb-activated sample, the maximum intensity (155295.21 cps) of the Pb^+ was obtained at the outmost surface. With the increasing in depth, the intensity of Pb^+ was also decreased. When the depth reached more than 1.8 nm, the Pb intensity became very stable and was only 10% of the initial intensity. Thus, it was expected that the thickness of PbS layer was nearly 1.8 nm. It was noticed that the thickness of Cu_2S layer was thicker than that of PbS layer for stibnite after treatment with $CuSO_4$ and $Pb(NO_3)_2$ at the same concentration. It appears that the adsorption capacity of Cu^{2+} was stronger than that of Pb^{2+} on stibnite surface. The solubility constant (K_{sp}) of Cu_2S is much lower than that of PbS in water (Adams et al., 2008; Zwiernik et al., 1998). For this reason, it is much easier to precipitate Cu_2S layer on the stibnite surface.

To investigate the distribution of copper or lead on the stibnite surface after the activation, 3D secondary ion images were reconstructed from the depth profile data, as shown in Fig. 8. It was observed that, at the Cu-activated surface, the surface was well coated by the Cu^+ ion and only limited amount of Cu^+ was found in the deeper layer from the top the surface, Fig. 8a. Differs from the Cu-activated surface, at the Pb-activated surface, the boundary between the active layer and the bulk phase of stibnite was less clear and a number of Pb^+ ions were found in the bulk of stibnite near to the surface, Fig. 8b. It appears that Pb^{2+} has a tendency to migrate into the bulk of stibnite and to bind with the S atom in the bulk.

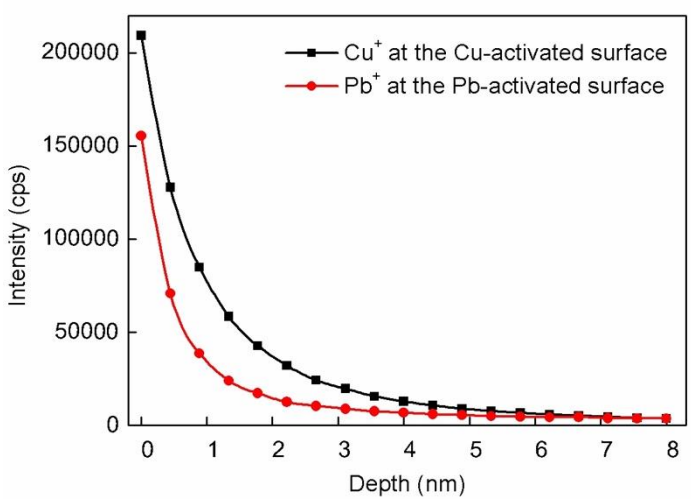

Fig. 7. Depth profiles of characteristic secondary ions in the positive mode for the stibnite treated with 5×10^{-5} mol/dm^3 of $CuSO_4$ or $Pb(NO_3)_2$

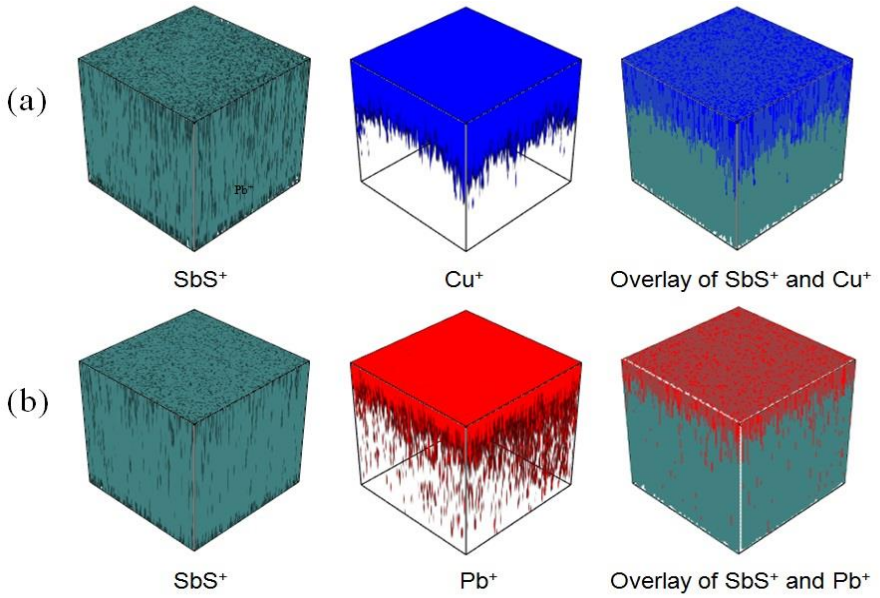

Fig. 8. 3D TOF-SIMS imaging of Cu-activated (a) and Pb-activated (b) stibnite surfaces (SbS^+=gray green, Cu^+=blue and Pb^+=red)

4. Conclusions

(1) With the addition of $CuSO_4$ or $Pb(NO_3)_2$, the stibnite recovery was improved with BX as a collector at the pH of 6.5.

(2) At the Cu-activated stibnite surface, Cu^{2+} was reduced to Cu^+ and further a Cu_2S layer was generated on the mineral surface. While, Pb^{2+} could also adsorbed on the stibnite surface to form a layer of PbS. The presence of Cu_2S or PbS layer at the stibnite surface improve the floatability of stibnite.

(3) With 5×10^{-5} mol/dm^3 of $CuSO_4$ or $Pb(NO_3)_2$, the thickness of Cu_2S layer and PbS layer on stibnite were reached about 2.8 nm and 1.7 nm respectively, which meet the requirement of the activation flotation of stibnite.

Acknowledgments

The financial support from National Science Foundation of China (No. 51304089) is gratefully acknowledged. The work was also supported by the Analysis and Testing Foundation of Kunming University of Science and Technology.

References

ADAMS, M., LAWRENCE, R., BRATTY, M., (2008), *Biogenic sulphide for cyanide recycle and copper recovery in gold–copper ore processing*, Minerals Engineering, 21, 509-517.

ALBERICI, S.G., ZONCA, R., PASHMOKOV, B., (2004), *Ti diffusion in chalcogenides: a ToF-SIMS depth profile characterization approach*, Applied Surface Science, 231, 821-825.

ANDERSON, C.G., (2012), *The metallurgy of antimony*, Chemie der Erde - Geochemistry, 72, 3-8.

CHELGANI, S.C., HART, B., (2014), *TOF-SIMS studies of surface chemistry of minerals subjected to flotation separation – A review*, Minerals Engineering, 57, 1-11.

CHELGNI, S.C., HART, B., XIA, L., (2013), *A TOF-SIMS surface chemical analytical study of rare earth element minerals from micro-flotation tests products*, Minerals Engineering, 45, 32-40.

DAI, Y.H., WANG, Q.L., ZHOU, H.Q., (2009), *Process Study on some Antimony Ore in Xinning of Hunan Province*, Hunan Nonferrous Metals, 25, 16-18.

HUANG, K., (1987), *The flotation behavior and surface electrical property of antimonite*, J. Cent.-South Inst. Min. Metall.(China), 1, 105-109.

JIANG, Y., YU, B.B., LIU, J., LI, Z.H., SUN, J.K., ZHONG, X., HU, J., SONG, W.G., WAN, L.J., (2015), *Boosting the Open Circuit Voltage and Fill Factor of QDSSCs using Hierarchically Assembled ITO@Cu2S Nanowire Array Counter Electrodes*, Nano Letters, 15, 3088-3095.

KHMELEVA, T.N., BEATTIE, D.A., GEORGIEV, T.V., SKINNER, W.M., (2013), *Surface study of the effect of sulphite ions on copper-activated pyrite pre-treated with xanthate*, Minerals Engineering, 16, 601-608.

LAGER, T., FORSSBERG, K.S.E., (1989), *Beneficiation characteristics of antimony minerals a review- part 1*, Minerals Engineering, 2, 321-336.

LAGER, T., FORSSBERG, K.S.E., (2015), *Comparative study of the flotation properties of jamesonite and stibnite*, Scandinavian Journal of Metallurgy, 18, 122-130.

LI, H., MU, S., WENG, X., ZHAO, Y., SONG, S., (2016), *Rutile flotation with Pb2+ ions as activator: Adsorption of Pb^{2+} at rutile/water interface*, Colloids and Surfaces A: Physicochemical and Engineering Aspects ,506, 431-437.

MAO, D., BLATZ, G., JR, C.E.W., GLOECKLER, M, (2016), *Correlative impurity distribution analysis in cadmium telluride (CdTe) thin-film solar cells by ToF-SIMS 2D imaging*, Solar Energy Materials & Solar Cells, 157, 65-73.

PENG, Y., GRANO, S., (2010), *Effect of grinding media on the activation of pyrite flotation*, Minerals Engineering, 23, 600-605.

SARVARAMINI, A., LARACHI, F., HART, B., (2016), *Collector attachment to lead-activated sphalerite – Experiments and DFT study on pH and solvent effects*, Applied Surface Science, 367, 459-472.

SOLOZHENKIN, P.M., ZINCHENKO, Z., KRILOVA, I., IVANOVA, N., (1991), *Flotation of complex antimony ore*, Proceedings of the 17th international conference on mineral processing, Dresden, Germany, pp. 163-174.

SUI, C.C., BRIENNE, S.H.R., XU, Z.H., FINCH J.A., (1997), *Xanthate adsorption on Pb contaminated pyrite*, International Journal of Mineral Processing, 49, 207-221.

THOMAS, J.P., ZHAO, L., ABDELLAH, M., HEINIG, N.F., LEUNG, K.T., (2013), *Interfacial micropore defect formation in PEDOT:PSS-Si hybrid solar cells probed by TOF-SIMS 3D chemical imaging*, Analytical Chemistry, 85, 6840-6845.

WANG, H., ZHOU, A., PENG, F., YU, H., YANG, J., (2007), *Mechanism study on adsorption of acidified multiwalled carbon nanotubes to Pb(II)*, Journal of Colloid & Interface Science, 316, 277-283.

XU, X., LIU, J.A., HU, X., (1991), *Non-chromate flotation separation of complex stibntie-cinnaber ore*, Nonferrous Metals, 1, 25-32.

ZWIERNIK, M.J., QUENSEN, J.F., BOYD, S.A., (1998), *$FeSO_4$ Amendments Stimulate Extensive Anaerobic PCB Dechlorination*, Environmental Science & Technology, 32, 3360-3365.